NANO LETTERS

2005
Vol. 5, No. 6
1065−1070

Controlling Plasmon Line Shapes through Diffractive Coupling in Linear Arrays of Cylindrical Nanoparticles Fabricated by Electron Beam Lithography

Erin M. Hicks, Shengli Zou, George C. Schatz, Kenneth G. Spears, and Richard P. Van Duyne*

Department of Chemistry, Northwestern University, 2145 Sheridan Road, Evanston, Illinois 60208

Linda Gunnarsson, Tomas Rindzevicius, Bengt Kasemo, and Mikael Käll

Department of Applied Physics, Chalmers University of Technology, S-412 96 Göteborg, Sweden

Received March 22, 2005; Revised Manuscript Received April 25, 2005

ABSTRACT

The effect of diffractive coupling on the collective plasmon line shape of linear arrays of Ag nanoparticles fabricated by electron beam lithography has been investigated using Rayleigh scattering spectroscopy. The array spectra exhibit an intricate multi-peak structure, including a narrow mode that gains strength for interparticle distances that are close to the single particle resonance wavelength. A version of the discrete dipole approximation method provides an excellent qualitative description of the observed behavior.

The unique size-dependent properties of nanomaterials have driven research in a multitude of fields, often leading to materials with important optical,[1] catalytic,[2] electronic,[3] and magnetic[4] properties. One of the most active areas of nanomaterials research is in applying the distinctive optical properties of noble metal nanoparticles for various applications such as chemosensors and biosensors.[4−6] The reason for the use of noble metal nanoparticles lies in their localized surface plasmon resonance (LSPR). The LSPR involves a collective oscillation of the conduction band electrons that arises in the metal nanoparticle when excited by a specific wavelength of electromagnetic radiation.[7] The position of this plasmon λ_{max} and the peak shape are determined by the shape, size, and composition of the particles as well as the interparticle distance and the external dielectric environment.[8−10]

Assemblies of nanoparticles often can be used to provide special functionalities that are important in sensing,[6] optical waveguides,[11] and filters.[12,13] The use of assemblies, rather than single particles, offers the ability to average a signal over several similar particles, thus increasing intensity and reducing discrepancies caused by defects. Since the design of a practical plasmonic nanodevice relies heavily on arrays of noble metal nanoparticles, the interactions between these nanoparticles is a crucial, and often overlooked, design parameter. These interactions, which include both short or long range contributions, are important for a variety of structure types, including both highly dense array structures[14,15] and individual pairs of nanoparticles.[16] The interactions can be measured and studied by observing changes in the LSPR peak shape and position. Theoretical calculations also show these unique interactions. For example, previous work by Schatz and co-workers has predicted narrowed plasmon peaks in one-dimensional[17] and two-dimensional arrays[18] as a result of diffractive interactions between the particles. For one-dimensional chains of particles above a critical size and with polarization and wave vectors taken to be perpendicular to the array axis, narrow peaks with widths less than 1 nm were predicted. The narrow peaks are caused by the coherent dipolar interactions between the particles when the incident wavelength is close in value to the interparticle distance.[17,19,20] Details of this mechanism, which involves rapid variation in the dipole sum as the wavelength is varied close to the interparticle separation, are described in ref 20. Because of radiative dipolar coupling between the particles (which varies as e^{ikr}/r), this interaction can be very long range, and the larger the array, the narrower the peak. By taking advantage of these coherent interactions, it is possible to create nanodevices with narrow lines that could

* Corresponding author. E-mail: vanduyne@chem.northwestern.edu.

10.1021/nl0505492 CCC: $30.25
Published on Web 05/18/2005

lead to better sensing capabilities than are possible with isolated metal particles or aggregates of particles.

Methods for preparing nanoparticle arrays vary as widely as their uses. Standard lithographic techniques can be broken into two major categories: direct-write methods and natural lithographies. Natural lithographies, including nanosphere lithography[21,22] and colloidial lithography,[23] are massively parallel and offer an inexpensive and rapid method for fabricating a large array of nanostructured materials. They, however, are limited by restricted lattice/interparticle spacings, shapes, and sizes that can be produced, as well as a large range of defects that occur in the structure. On the other hand, direct-write methods, such as electron beam lithography (EBL),[24] focused ion beam (FIB) milling,[25] and dip-pen lithography,[26] offer fine control of size, shape, and lattice spacing, as well as few defects. Of the major problems associated with direct-write methods are the serial nature of the process and the higher cost associated with production of arrays. EBL was chosen for this project because fine-control over sample morphology was crucial (based on theoretical modeling) to whether the coherent diffractive coupling was going to be observed.

This work presents experimental evidence for the effects of diffraction on plasmon line shapes predicted by theory, using lines of silver particles fabricated with EBL. A critical factor in producing this effect is the uniformity of the all the particles and the straightness of the linear array. EBL readily lends itself to precision control of nanoparticle features and particle spacing, which is ideal for studying the plasmon narrowing. Because the experimental parameters used were different than in the original theoretical study,[17] an extension of the theoretical work is also presented.

Nanoparticle arrays were prepared by EBL on number 2 cover glass slips (Fisher Scientific, Pittsburgh, PA). The resolution of the EBL system used (JEOL JBX5D-II, JEOL, Japan) is approximately 20 nm, employing an accelerating voltage of 50 kV. The rest of the preparation follows a published procedure.[24] ZEP 520 (dilute 1:2 anisole, Nippon Ltd, Japan) was spun onto the glass cover slips and 10 nm of Au was deposited prior to exposure in the EBL. After exposure, the Au film was removed by etching and the patterns were then developed in hexyl acetate. Ag was thermally deposited (AVAC HVC600) over both the pattern and resist and subsequently removed, leaving patterned nanoparticles behind. This was accomplished by slightly over-developing the resist. In this work each array contained columns of 500 particles and, because of this, the sizes of the arrays varied depending on the interparticle spacing.

The theoretical predictions involved particles in a homogeneous medium rather than on a substrate. To reproduce this environment, the particles were sandwiched between two glass cover slips, with Nikon oil in between (RI = 1.5). All optical measurements were made using an inverted microscope (Eclipse TE300, Nikon Instruments) with a fiber coupled to a miniature grating spectrometer (AvaSpec 2048, Avantes). The scattering measurements reported here were recorded over the range 350−850 nm. White light from the TE300 lamp was polarized before being passed through a dark-field condenser (NA = 0.7−0.85) that was used to excite the nanoparticle arrays. The scattered light was collected with a 60× (NA = 0.7) objective. A color video camera was also attached to the front port to collect optical images of the particle columns.

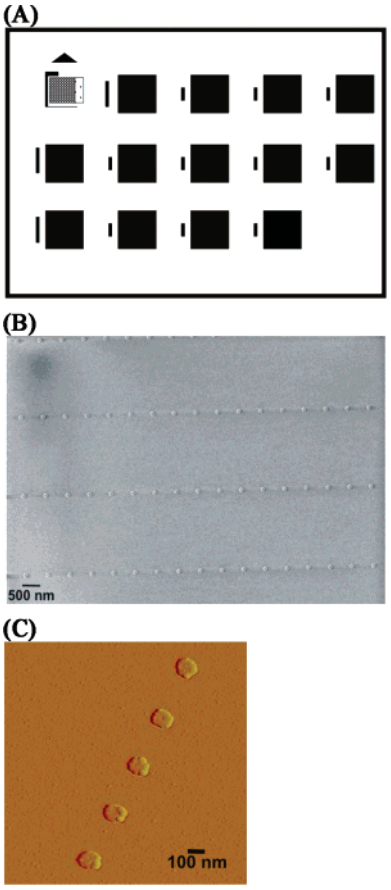

Figure 1. (A) Schematic of overall sample layout. Multiple lines of the same spacing were combined to create pads of particles (black squares). The pads were arranged in increased interparticle spacing, and the first pad contained a single-particle pad. (B) SEM image taken of a particle pad on glass with an interparticle spacing of 632 nm, diameter = 130 nm, height = 30 nm. (C) AFM image of a few Ag nanoparticles on glass. Height = 31.33 ± 1.3 nm, width = 133 ± 4.3 nm.

Characterization of the morphology of the samples was conducted with both atomic force microscopy (AFM) and scanning electron microscopy (SEM). AFM images were collected using a Digital Instruments Nanoscope III microscope (Digital Instruments, Santa Barbara, CA) operated in tapping mode with asymmetric phosphorus n-doped Si nanoprobe tips (Veeco, Santa Barbara, CA). These tips have resonance frequencies between 305 and 370 kHz and are conical shape with an effective radius of curvature at the tip of 10 nm. SEM images were obtained using a Gemini LEO Ultra 55 (Carl Zeiss SMT AG, Germany), with an accelerating voltage of 1 keV and an average working distance of 4 mm.

Sample preparation is a critical step in being able to observe the "diffractively narrowed plasmon". Using EBL was a logical choice because samples could be easily made with multiple spacings on a single substrate (Figure 1A). EBL also produces minimal defect arrays (Figure 1B and 1C). Figure 1A shows a general layout for the overall

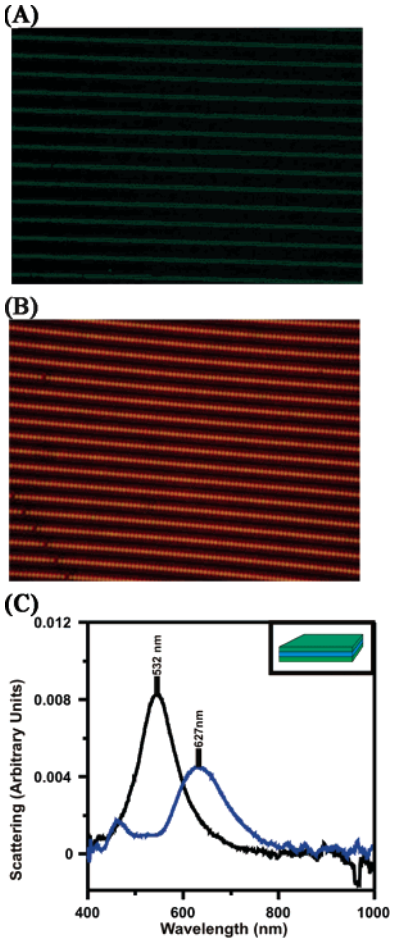

Figure 2. (A) Dark-field image of lines of particles before the uniform refractive index structure is placed around the particles. The line spacing is 5 μm and the particle diameter is 100 nm. (B) Dark-field image of lines of particles after index matching is applied, causing the red shift in color. Line spacing is 2 μm and particle diameter is 130 nm. (C) Single-particle plasmon taken from the sample both with (blue solid line) and without (black solid line) index matching. The particle dimensions are as follows: height = 30 nm, diameter = 100 nm. Inset is a depiction of how uniform RI was achieved with the nanoparticles surrounded by two layers of glass (green) and an index matched oil (blue).

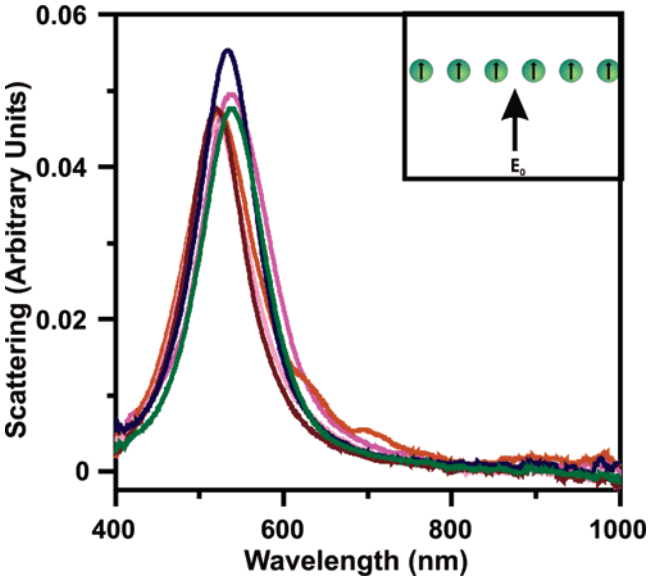

Figure 3. Plasmon spectra for the linear arrays before any uniform refractive index was created surrounding the particles. This selected set of spectra correspond to interparticle spacings of 300, 400, 500, 600, 700, and 800 nm. For clarity, spectra for the other spacings were omitted. No sharp plasmonic shoulder is seen. Inset shows the optical excitation geometry.

substrate design. To make finding the particles on the substrate easier, several markers were created far enough away to eliminate any interactions, but close enough to find the particles (triangle and vertical rectangles in Figure 1A). Each substrate is made up of pads consisting of columns of particles of various spacing. Large areas of each spacing were fabricated to increase the signal from a specific spacing. The distance between columns was varied from 2 μm to 10 μm to minimize coupling, and take advantage of the predicted narrower line shapes for one-dimensional compared to two-dimensional arrays. Each pad was separated by 2 mm, optically isolating each pad. Included on each substrate is also a pattern of particles spaced 5 μm to obtain a single particle spectrum for each sample. In Figure 1B and 1C, the particle uniformity can be seen. The cylindrical nanoparticles have an average height of 30 nm, and width of either 100 or 130 nm, depending on the sample type. Also, in Figure 1B the straightness of the columns can be seen. In larger field views (data not shown) the columns are continuous over long distances with few defects making them ideal for studying diffractive coupling effects.

Figures 2A and 2B show the optical uniformity of the samples produced by EBL. Each of the particles is the same color, blue-green, before refractive index (RI) matching, and red-orange afterward. The red shift seen in the two images is due to the greater RI of the matched sample glass/oil/glass, RI = 1.5/1.5/1.5, (Figure 2B) versus the unmatched glass/air sample, RI = 1.5/1.0, (Figure 2A). The optical micrograph also shows that the separation between columns of particles eliminates any major coupling, as evidenced by the void space between the fields that surround each column. The inset in Figure 2A illustrates the excitation geometry of the particles. Figure 2C shows representative single-particle plasmon spectra for the samples used in this study. The single-particle spectrum was obtained using EBL-produced cylindrical particles spaced 5 μm apart from each other in both air and oil with another cover slip on top.

After preliminary optical and physical characterizations of the samples were conducted, to ensure high sample quality, the nonindexed matched plasmon was investigated for each interparticle distance (Figure 3). The λ_{max} for the spacings tested all vary around a peak position of 525 nm and have a full width half-maximum (fwhm) of 90 nm. Thus the spectra have narrow uniform peaks, but without the dependence on interparticle spacing that would be a signature of diffractive coupling. The reason for this is simply that the speed of light is different above (air) and below (glass) the particles, preventing an effective coherent coupling between adjacent particles.

Figure 4 shows that for the index matched samples, there is a shoulder on the red side of the single particle plasmon, whose wavelength varies with particle spacing. The particles in Figure 4A have a diameter of 130 nm and a height of 30

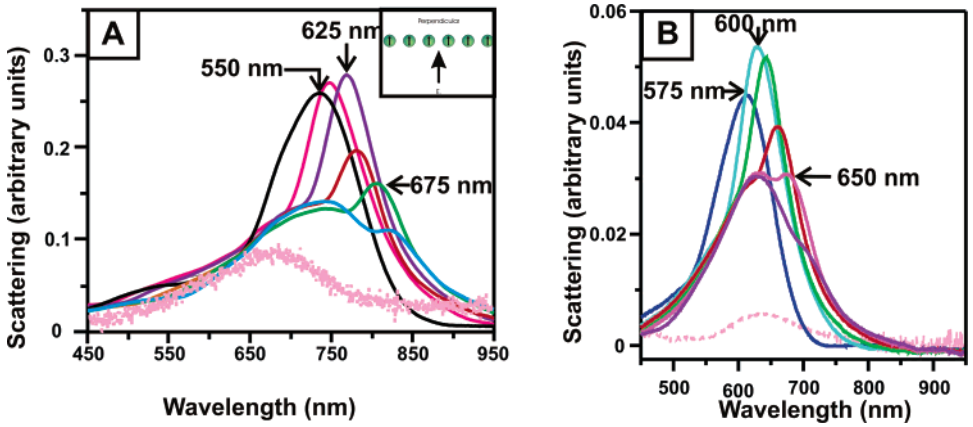

Figure 4. (A) and (B) show the darkfield measurements for samples with 2 and 5 μm interline spacing and cylinder diameters of 130 and 100 nm, respectively, taken of arrays varying in interparticle spacing from 400 to 700 nm with a uniform refractive index (RI = 1.5) around the particles. Both (A) and (B) were collected with a 60× objective. The optical excitation geometry for (A) and (B) is the same as the inset seen in Figure 3. The corresponding single particle spectra are shown (dotted line in A and dashed line in B) with peak positions of λ_{max} = 660 nm in (A) and λ_{max} = 627 nm in (B).

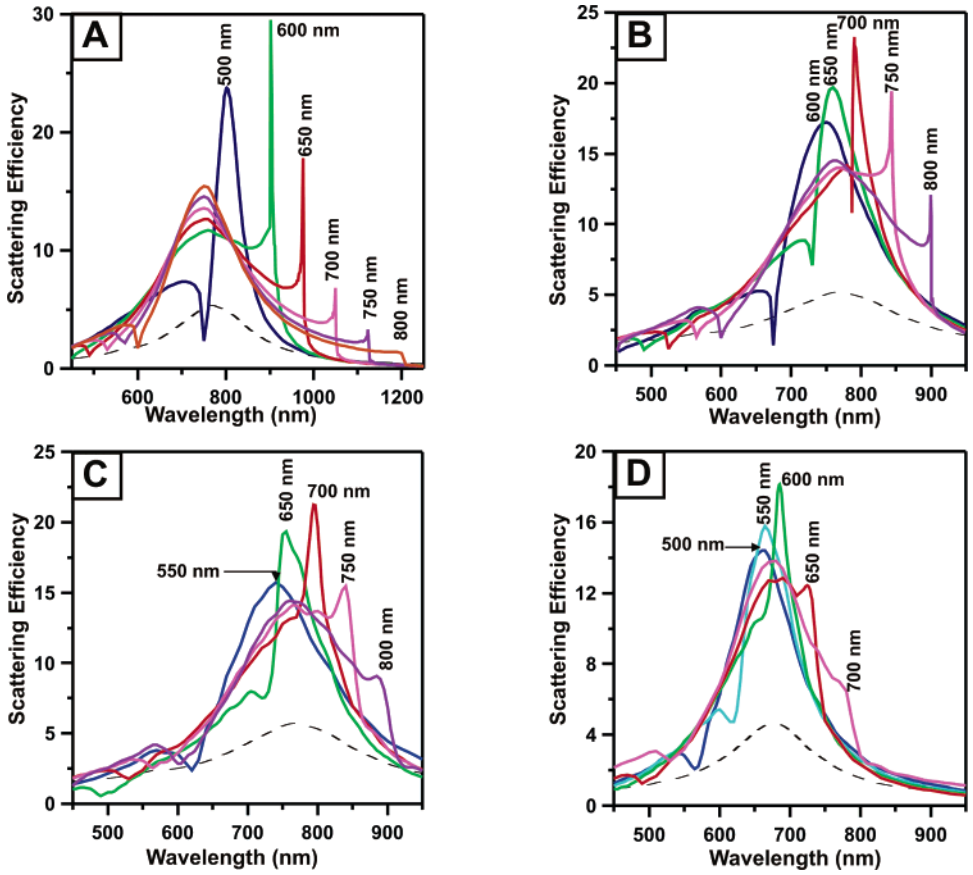

Figure 5. (A) Scattering efficiencies for a chain of 500 cylinders with height of 30 nm and diameter of 130 nm with an incident angle of 0 degrees (normal incidence). (B) Scattering efficiencies for a chain of 500 cylinders with height of 30 nm and diameter of 130 nm with an incident angle of 30 degrees. (C) Scattering efficiencies for a chain of 20 cylinders with height of 30 nm and diameter of 130 nm with a 30 degrees incident angle. (D) Scattering efficiencies for a chain of 20 cylinders with height of 30 nm and diameter of 100 nm with a 30 degrees incident angle. Corresponding single particle spectra for each case are included (dashed line). The single particle spectra have been scaled by a factor of 2.

nm, and for a separation of 550 nm, the peak has low intensity and fwhm of approximately 125 nm. As the interparticle distance increases toward the single particle resonance wavelength, the shoulder on the red portion of the line shape narrows and becomes more intense, with a maximum intensity occurring at a spacing of 625 nm (fwhm = 60 nm). For still larger spacings, the peak remains narrow, but decreases in intensity until it is no longer observed in the spectrum. The narrow shoulder also occurs in arrays with larger column spacings (5 μm) and slightly smaller particles (100 nm), as seen in Figure 4B. The progression of plasmon peaks is the same as above: below the optimal spacing the

plasmon peak is low in intensity and broad (fwhm = 100 nm, 525 nm spacing), at the optimal spacing of 600 nm there is a shoulder whose fwhm is 50 nm, and above the optimal spacing the shoulder decreases in intensity and eventually disappears altogether. The spectra in 4B are blue shifted from those in 4A due to the smaller particle size. When collecting with other objectives (i.e. 10×), the property can still be seen (data not shown).

In the earlier theoretical study,[17] only the extinction spectra were calculated. Because of the weak signals produced by the arrays it was necessary to use Rayleigh scattering spectroscopy rather than extinction, so in the present studies we have calculated the scattering spectra for one- and two-dimensional arrays of silver nanoparticles to simulate the measurements. First, the periodic discrete dipole approximation DDA method described previously[27−30] was used to generate results for two-dimensional rectangular arrays of 130 nm diameter particles each with height 30 nm and with a 2 μm distance between each column. The results for a spacing of 600 nm (not shown) were compared with the one-dimensional chain results, and only small differences were found, so additional calculations only considered the one-dimensional chains. The additional calculations involve varying the interparticle distance from 500 to 800 nm, with a cylinder height of 30 nm and particle diameter of either 100 or 130 nm. The calculations considered 500 particles in which both polarization and wave vectors are perpendicular to the array axis. The index of refraction of the medium is taken to be 1.5. We first carried out calculations for normal incidence. The results for the 130 nm particles are presented in Figure 5A, along with the corresponding single-particle spectrum. The figure shows resonance peaks at longer wavelength than the experimental results. We then carried out the same calculations with an incident angle of 30°. The results for the 130 nm particles are presented in Figure 5B, along with the corresponding single-particle spectrum. The figures show resonance wavelengths and variation with spacing that are in qualitative agreement with the observations. However, the shoulder on the red portion of the plasmon band is much narrower than in the experiments, with widths as small as 2 nm when the interparticle spacing is 750 nm. Figure 5C shows that if only adjacent groups of 20 particles in the 500 particle chain are allowed to couple, the widths are in more reasonable agreement with the measured results in Figure 4A. Figure 5D shows analogous results for the 100 nm diameter particle, and again we see that the results when only 20 adjacent particles are allowed to couple (Figure 5D) match the experiments in Figure 4B reasonably well. The good agreement for reduced coherent coupling between the particles likely mimics the influence of the spread in illumination and collection angles in the experiment, which smear the strict scattering configuration assumed in the theoretical simulation. It is also possible that defects, lattice imperfections, the incoherent light source and local variations in the index of refraction contribute to the broadening, and indeed we note that even in Figure 5C and 5D there is more structure in the calculations than is seen in the experiments, particularly for the dip in the line shapes at wavelengths to the blue of the single-particle plasmon wavelength. This dip, whose origin is explained in ref 19, is more easily obscured by broadening effects and thus is less likely to be observed given the significant broadening that we find in the experimental results.

In summary, this work demonstrates that it is possible to significantly affect plasmon line shapes in linear arrays of cylindrical particles through diffractive coupling, following up the earlier predictions of theory.[17] Critical factors to the success of this experiment are the use of a dark field light scattering, a uniform refractive index, and high sample quality. By varying the interparticle spacing from 350 to 800 nm, the diffractively induced peak grows into the plasmon spectrum, reaches a maximum, and then decreases in intensity and eventually disappears. Also presented are theoretical calculations that support the experimental data. EBL has provided the ideal tool to make multiple sample areas on a substrate with precise control over particle size and spacing. By showing experimental evidence for diffractive control of plasmon line shapes, the design of new schemes to further improve the diffractive response should be possible.

Acknowledgment. Funding for this work was provided by NSEC program of the NSF (EEC-0118025), the Air Force Office of Scientific Research MURI program (F49620-02-1-0381), the National Science Foundation (DMR-0076097), the Swedish Research Council (contract no. 2001-2672), and the Photonano Program of the Swedish Foundation for Strategic Research (A3 O2:143). The authors acknowledge Dr. Christy Haynes for initiating the collaboration between the groups to make this work possible. E.H. thanks Dr. Yury Alaverdyan, Ms. Katarina Logg, and Mrs. Chanda R. Yonzon for the help and valuable discussions.

References

(1) Kreibig, U.; Vollmer, M. *Metal Clusters*; Springer-Verlag: Heidelberg, Germany, 1995; p 532.
(2) Street, S. C.; Xu, C.; Goodman, D. W. *Annu. Rev. Phys. Chem.* **1997**, *48*, 43−68.
(3) Andres, R. P.; Bielefeld, J. D.; Henderson, J. I.; Janes, D. B.; Kolagunta, V. R.; Kubiak, C. P.; Mahoney, W. J.; Osifchin, R. G. *Science* **1996**, *273*, 1690−1693.
(4) Shi, J.; Gider, S.; Babcock, K.; Awschalom, D. D. *Science* **1996**, *271*, 937−941.
(5) Storhoff, J. J.; Elghanian, R.; Mucic, R. C.; Mirkin, C. A.; Letsinger, R. L. *J. Am. Chem. Soc.* **1998**, *120*, 1959−1964.
(6) Riboh, J. C.; Haes, A. J.; McFarland, A. D.; Yonzon, C. R.; Van Duyne, R. P. *J. Phys. Chem. B* **2003**, *107*, 1772−1780.
(7) Haes, A. J.; Van Duyne, R. P. *J. Am. Chem. Soc.* **2002**, *124*, 10596−10604.
(8) Schatz, G. C.; Van Duyne, R. P. Electromagnetic Mechanism of Surface-Enhanced Spectroscopy. In *Handbook of Vibrational Spectroscopy*; Chalmers, J. M., Griffiths, P. R., Eds.; Wiley: New York, 2002; Vol. 1, pp 759−774.
(9) Lamprecht, B.; Schider, G.; Lechner, R. T.; Ditlbacher, H.; Krenn, J. R.; Leitner, A.; Aussenegg, F. R. *Phys. Rev. Lett.* **2000**, *84*, 4721−4724.
(10) Jensen, T.; Kelly, L.; Lazarides, A.; Schatz, G. C. *J. Cluster Sci.* **1999**, *10*, 295−317.
(11) Knoll, W. *Annu. Rev. Phys. Chem.* **1998**, *49*, 569−638.
(12) Barnes, W. L.; Dereux, A.; Ebbesen, T. W. *Nature* **2003**, *424*, 824−830.
(13) Ebbesen, T. W.; Lezec, H. J.; Ghaemi; H. F.; Thio, T.; Wolff, P. A. *Nature* **1998**. *391*, 667−669.
(14) Haes, A. J.; Zou, S. L.; Schatz, G. C.; Van Duyne, R. P. *J. Phys. Chem. B* **2004**, *108*, 109−116.

(15) Haes, A. J.; Zou, S. L.; Schatz, G. C.; Van Duyne, R. P. *J. Phys. Chem. B* **2004**, *108*, 6961−6968.
(16) Gunnarsson, L.; Rindzevicius, T.; Prikulis, J.; Kasemo, B.; Käll, M.; Zou, S. L.; Schatz, G. C. *J. Phys. Chem. B* **2005**, *109*, 1079−1087.
(17) Zou, S.; Janel, N.; Schatz, G. C. *J. Chem. Phys.* **2004**, *120*, 10871−10875.
(18) Zou, S.; Schatz, G. C. *J. Chem. Phys.* **2004**, *121*, 12606−12612.
(19) Zou, S.; Schatz, G. C. *SPIE Proc.* **2004**, *5513*, 22−29.
(20) Zou, S.; Schatz, G. C. *J. Chem. Phys.* **2005**, in press.
(21) Haynes, C. L.; Van Duyne, R. P. *J. Phys. Chem. B* **2001**, *105*, 559−5611.
(22) Hulteen, J. C.; Van Duyne, R. P. *J. Vac. Sci. Technol. A* **1995**, *13*, 1553−1558.
(23) Hanarp, P.; Käll, M.; Sutherland, D. S. *J. Phys. Chem. B* **2003**, *107*, 5768−5772.
(24) Haynes, C. L.; McFarland, A. D.; Zhao, L. L.; Schatz, G. C.; Van Duyne, R. P.; Gunnarsson, L.; Prikulis, J.; Kasemo, B.; Käll, M. *J. Phys. Chem. B* **2003**, *107*, 7337−7342.
(25) Tong, H. D.; Jansen, J. V.; Gadgil, V. J.; Bostan, C. G.; Berenschot, E.; van Rijn, C. J. M. *Nano Lett.* **2004**, *4*, 283−287.
(26) Piner, R. D.; Zhu, J.; Xu, F.; Hong, S.; Mirkin, C. A. *Science* **1999**, *283*, 661−663.
(27) Draine, B. T.; Flatau, P. J. U*ser Guide for the Discrete Dipole Approximation Code DDSCAT.6.0*; 2003.
(28) Draine, B. T.; Flatau, P. J. *J. Opt. Soc. Am. A* **1994**, *11*, 1491.
(29) Kelly, K. L.; Coronado, E.; Zhao, L.; Schatz, G. C. *J. Phys. Chem. B* **2003**, *107*, 668.
(30) Zhao, L. L.; Kelly, K. L.; Schatz, G. C. *J. Phys. Chem. B* **2003**, *107*, 7343−7350.

NL0505492